Elsevier Editorial System(tm) for European Polymer Journal

Manuscript Draft

Manuscript Number:

Title: Probing the chain segment mobility at the interface of semi-crystalline polylactide/clay nanocomposites

Article Type: Research Paper

Section/Category: Regular Paper

Keywords: PLA, nanocomposite, exfoliated, crystalline fractions, chain mobility, cooperativity

Corresponding Author: Dr. ALLISSON SAITER,

Corresponding Author's Institution: AMME-LECAP international laboratory EA4528

First Author: ALLISSON SAITER

Order of Authors: ALLISSON SAITER; Nicolas Delpouve; Eric Dargent; Werner Oberhauser; Lucia Conzatti; Francesca Cicogna; Elisa Passaglia

Abstract: The concept of cooperative rearranging region (CRR), an efficient probe of the interaction level in nanocomposites, has been used in Poly(lactic acid) (PLA)-based composites with phyllosilicates prepared in the melt with organomontmorillonite (O-MMT) and using poly(butylene adipate-co-terephthalate) (PBAT) as coupling agent. The samples were crystallized from various thermal treatments in order to obtain a wide range of morphologies and microstructures and accurately characterized by XRD, TEM, standard DSC and MT-DSC with the aim to highlight the effect of lamellae dispersion and distribution at nanoscale onto the thermal features of resulting nanocomposites. The presence of different interaction levels at the interface PLA/O-MMT, even tuned by the presence of PBAT, affects both the crystalline phase structure (by differently promoting crystallization of alpha and alpha' forms) and the distribution between the amorphous fractions (rigid and mobile). The variations of molecular dynamics are classified in two categories depending on the composite microstructure. Only in amorphous materials the cooperativity is driven by the filler/matrix interactions. In semi-crystalline materials, the morphological features linked to the presence of O-MMT and PBAT are overwhelmed by the confinement of the amorphous phase. Comparison between the two crystallization modes evidences a stronger change in the glass transition dynamics for systems exhibiting preponderant nucleation and high percentage of rigid amorphous fraction.

Suggested Reviewers: Christoph Schick
christoph.schick@uni-rostock.de

Sabu Thomas
sabuchathukulam@yahoo.co.uk

Giovanni Camino
giovanni.camino@proplast.it

Vikas Mittal
vmittal@pi.ac.ae

Suprakas Sinha Ray
rsuprakas@csir.co.za

Dr Allisson SAITER
AMME-LECAP EA4528 International Laboratory,
Université et INSA de Rouen,
BP12, 76801 Saint Etienne du Rouvray Cedex, France
tel: 00.33.2.32.95.50.86
fax: 00.33.2.32.95.50.82
allison.saiter@univ-rouen.fr

7th January 2016

Dear Editor,

Please find our article entitled "Probing the chain segment mobility at the interface of semi-crystalline polylactide/clay nanocomposites" for a submission into European Polymer Journal.

This paper reports new experimental results focused on polylactide/clay nanocomposites using PBAT as coupling agent. The samples have been accurately characterized by different experimental techniques: XRD, TEM, TGA, standard DSC and MT-DSC with the aim to highlight the effect of lamellae dispersion and distribution at nanoscale onto the thermal features of resulting nanocomposites. We show that the presence of different interaction levels at the interface PLA/O-MMT, even tuned by the presence of PBAT, affects both the crystalline phase structure (by differently promoting crystallization of α and α' forms) and the distribution between the amorphous fractions (rigid and mobile). Furthermore, we show that the cooperativity degree obtained from MT-DSC is a powerful complementary tool to X-Ray diffraction and microscopy when investigating the morphology of nanocomposites since it probes the physical interactions between the matrix and the filler. When the dominant morphology of the nanocomposite is exfoliated, the interfacial interactions between the matrix and the filler increase the cooperativity. On the other hand, intercalated morphology renders less effective the formation of physical bonds due to the confinement of the macromolecules in the galleries of fillers, decreasing hence the cooperativity degree.

As far as we know, the study of the combined influence of the morphological dependence and the confinement dominance on the cooperativity degree doesn't exist in the literature.

Sincerely,

Dr. Allisson SAITER

UNIVERSITE DE ROUEN
AMME-LECAP International Laboratory
Avenue de l'Université – CS70012,
76801 St Etienne du Rouvray Cedex – France
Tél. : 33(0)2.32.95.50.81 - Fax : 33(0)2.32.95.50.82

*Graphical Abstract

How the cooperativity length changes with structure ?

Cooperativity length

Intermolecular interactions

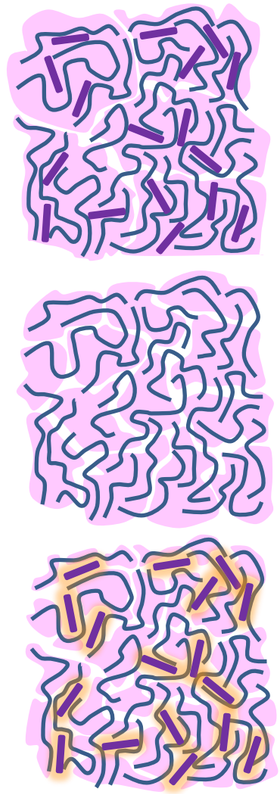

Morphological dependence

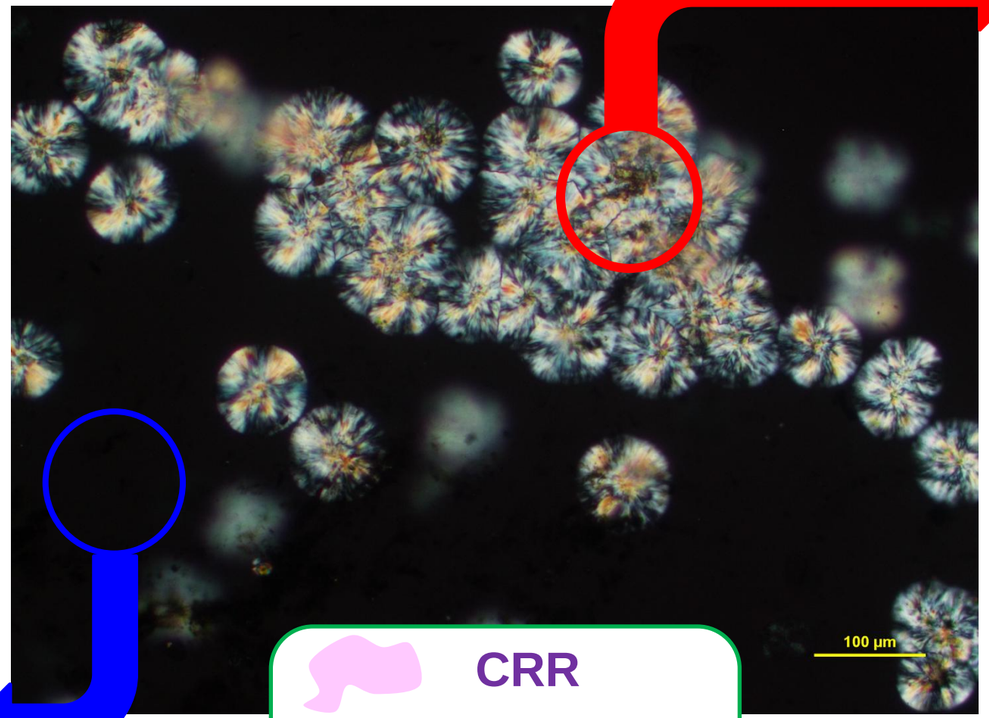

CRR

O-MMT

PBAT

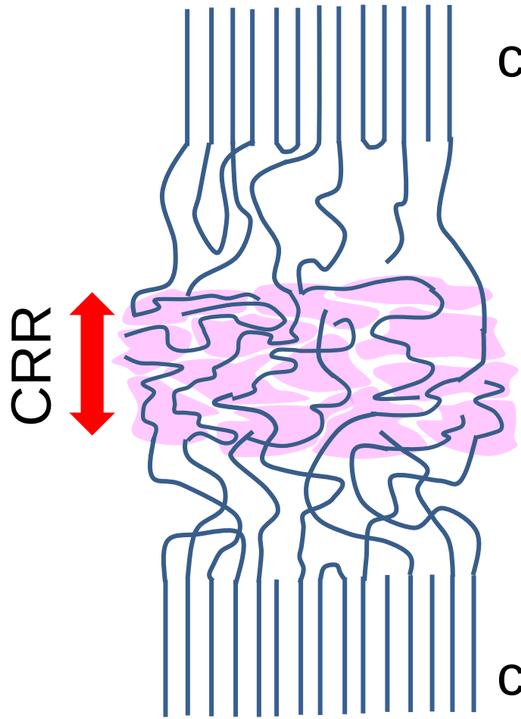

Confinement dominance

Highlights:

1) Further deepening in interfacial properties of PLA nanocomposites with organo-clay
2) Role of PBAT in morphology evolution and polymer chain mobility
3) The level of interactions in the nanocomposites was probed using the CRR concept
4) Higher degree of cooperativity in exfoliated structures compared to intercalated ones
5) In semi-crystalline samples, the interaction level is independent on the morphology.

Probing the chain segment mobility at the interface of semi-crystalline polylactide/clay nanocomposites

A. Saiter[1*], N. Delpouve[1], W. Oberhauser[2], L. Conzatti[3], F. Cicogna[4], E. Passaglia[4*]

[1]*AMME-LECAP EA 4528 International Lab., Av. de l'Université, BP12, Normandie Univ. France, Université de Rouen, 76801 St Etienne de Rouvray, France*

[2]*ICCOM-CNR Firenze,Via Madonna del Piano 10, 50019 Sesto Fiorentino, Firenze, Italy*

[3]*ISMAC-CNR Genova, via De Marini 6 16149 Genova, Italy*

[4]*ICCOM- CNR UOS Pisa, Via G. Moruzzi 1, 56124 Pisa, Italy*

*corresponding authors: allison.saiter@univ-rouen.fr ; passaglia@pi.iccom.cnr.it

Abstract

The concept of cooperative rearranging region (CRR), an efficient probe of the level of interactions in nanocomposites, has been used in Poly(lactic acid) (PLA)-based composites with phyllosilicates prepared in the melt with organomontmorillonite (O-MMT) and using poly(butylene adipate-co-terephthalate) (PBAT) as coupling agent. The samples were crystallized from various thermal treatments in order to obtain a wide range of morphologies and microstructures and accurately characterized by XRD, TEM, standard DSC and MT-DSC with the aim to highlight the effect of lamellae dispersion and distribution at nanoscale onto the thermal features of resulting nanocomposites. The presence of different interaction levels at the interface PLA/O-MMT, even tuned by the presence of PBAT, affects both the crystalline phase structure (by differently promoting crystallization of α and α' forms) and the distribution between the amorphous fractions (rigid and mobile). The variations of molecular dynamics are classified in two categories depending on the composite microstructure. Only in amorphous materials the cooperativity is driven by the filler/matrix interactions. In semi-crystalline materials, the morphological features linked to the presence of O-MMT and PBAT are overwhelmed by the confinement of the amorphous phase. Comparison between the two crystallization modes evidences a stronger change in the glass transition dynamics for systems exhibiting preponderant nucleation and high percentage of rigid amorphous fraction.

Keywords

PLA, nanocomposite, exfoliated, crystalline fractions, chain mobility, cooperativity

Introduction

The key parameter in obtaining reinforced material by adding fillers is the interactions between the constituents. The interactions at interface between the materials forming the composite structure might involve multiple types of bonds depending upon the structure of the additive used with the matrix polymer. Usually these interactions are difficultly quantifiable as the structural description of the composite is restricted to its morphology obtained from X-ray diffraction and to the homogeneity of the filler dispersion obtained from electronic microscopy. However, during the last ten years many studies [1] [2] [3] [4] [5] [6] [7] [8] have correlated the level of interactions at the interface between the filler and the matrix to the average size of one domain relaxing at the glass transition or Cooperative Rearranging Region (CRR) [9]. This idea of Cooperative Rearranging Region (CRR), which is defined as the amorphous domain where a conformational rearrangement may occur without causing rearrangements in the surrounding, has been introduced by Adam and Gibbs [9] and has given birth to many approaches aiming at calculating the characteristic length of the glass transition. Among them there is the thermodynamic approach proposed by Donth [10] which relates the CRR to the dynamic heterogeneity deduced from the temperature fluctuation associated with the glass transition. This approach provides a picture of the relaxation time at the glass transition which is directly observable through calorimetric measurements [11] and has been widely used to analyze the molecular mobility in amorphous domains of complex systems at the glass transition [12] [13] [14] [15] [16] [17]. An increasing number of studies relate the degree of cooperativity to the number and ratio of weak physical inter-chain bonds [15] [18] [19] [20] [21] [22]. Furthermore, it is speculated that, in nanoconfined environments, the exfoliated nanoclays can anchor polymer chains leading to a cooperativity increase [1] [5], whereas in intercalated morphologies the macromolecules are confined in the galleries of clays [3] [5] [7], leading to a decrease of the cooperativity. However the number of studies considerably reduces when the systems contain other additives than the filler, with additional structural heterogeneities induced by microstructure changes, although these procedures are common in industry.

As an example, poly(lactic acid) (PLA) is a biodegradable, linear, aliphatic poly-ester, produced from renewable resources and thus its use is appealing for different industrial applications. Even though PLA has numerous advantages such as being eco-friendly and

having high strength and modulus; being intrinsic brittle, having low heat distortion temperature, showing high gas and vapor permeability, and exhibiting poor resistance to protracted processing operations have strongly limited its applications and restrict its utilization in pristine form, particularly for packaging uses. Similar to the conventional plastics, PLA-based composites made by employing inorganic or natural fillers are the potential methods to improve its mechanical properties and even its functional features. Reinforcement of biodegradable polymers through the addition of macro or nano-scale reinforcements can be a useful method in production of eco-friendly nanocomposites for various applications [23][24]. With reference to layered inorganic systems both montmorillonite (MMT) and layered double hydroxides as hydrotalcite (LDH) have been used to provide PLA based nanocomposites. In both cases the use of suitable surfactants (ionic salts used as organomodifiers) is necessary to promote interactions, to enlarge the intergalleries spacing and to provide morphologies suitable to reach the target features (mechanical improvements and/or barrier properties) [25][26][27][28]. In addition, in some cases, a reactive coupling agent or polymer compatibilizer were employed [29][30].

In order to better characterize the structure of PLA-based nanocomposites, the thermal analysis is a very useful tool [31]. While their thermal stability is well characterized by means of thermogravimetric analysis (TGA), the differential scanning calorimetry (DSC) investigations have been used in order to determine not only the characteristic temperatures as the glass transition temperature, the cold crystallization temperature and the melt temperature, but also the enthalpies of melting and crystallization, and then the crystallinity degree. As an example, in ref. [32], W. S. Chow et al. examined the effects of the organo-montmorillonite (O-MMT 1% w/w) and the maleic anhydride-grafted ethylene propylene rubber (EPMgMA) as compatibilizer, on the thermal properties of PLA by using TGA and DSC. They showed that the thermal stability of PLA_O-MMT was greatly enhanced by the addition of EPMgMA. Furthermore, the crystallinity degree of the PLA was increased by the O-MMT incorporation, and conversely reduced by EPMgMA addition. They showed that even the crystallization temperature of PLA was decreased by adding both O-MMT and EPMgMA. Recently, A. K. Mohapatra et al. [29] studied the thermal behavior of nanocomposites based on PLA/ poly(butylene adipate-co-terephthalate) (PBAT) blends with cloisite 30B as nanofiller provided by a reactive blending procedure employing maleic anhydride and peroxide to promote efficient PLA/PBAT interfacial interactions. Very similar approach was used by M. Kumar et al. [31] by using glycidyl methacrylate (GMA) as reactive compatibilizer. Thermo-

mechanical and morphological investigations showed the improvement of the final properties of nanocomposites as compared with virgin PLA, even if the role of PBAT and reagents onto the confinement effects were not fully investigated.

The goal of this work is also to investigate by DSC the influence of the crystalline phase on the chain segment mobility in PLA_O-MMT nanocomposites, obtained by dispersing O-MMT even in the presence of PBAT, used here as surfactant/compatibilizer in a very low amount. The materials have been analyzed as formulated, then annealed with different procedures generating the α and/or α' crystalline forms [33]. The results obtained in terms of chain segment mobility were compared to the experimental results obtained by XRD and TEM, all aimed at investigating the starting morphology of PLA nanocomposites. In addition, to understand how the PBAT interferes with the morphology of PLA_O-MMT nanocomposites, we carried out modulated temperature DSC (MT-DSC) experiments in order to estimate the degree of cooperativity at the glass transition as a probe of the chain segment mobility. Indeed, recent works have validated this approach to obtain a structural representation of the physical interaction landscape in a material which undergoes structural hindrances [34], including the addition of nanofillers [35].

Materials and methods

Materials

Poly(lactic acid) PLA 2002D, 96% L-lactic acid (PLA) supplied by NatureWorks®, (Minnetonka, MN, USA) [melt flow index (MFI) (2.16 kg, 190°C) 4–8 g $(10\ min)^{-1}$], was used as the polymer matrix. Before processing, PLA was dried in a vacuum oven at 110 °C for 18 h.

Poly(butylene adipate co-terephthalate) (PBAT) supplied by BASF is a copolymer containing 45.5 % mol of terephthalate used as compatibilizer. It is characterized by number average molecular weight (Mn) = 26400 D and weight average molecular weight (Mw) = 50800 D.

The clay (O-MMT) is a phyllosilicate, a commercial product from Laviosa Chimica Mineraria Chemicals with trade name Dellite 43B. It is an organophilic montmorillonite modified with dimethyl benzyl hydrogenated tallow ammonium salt; the nominal content of surfactant (ammonium salt) as reported by the data sheet of provider is 36% w.

Sample preparation

The preparation of all the samples has been carried out in a discontinuous mechanical mixer Brabender (Plastograph OHG47055, 30 mL chamber) at 180 °C for 15 min and setting a rotor speed of 60 rpm. The amount of polymer introduced was for all the runs 20 g (PLA and eventually PBAT) and the filler was added after 3 minutes. During the runs the Torque values were monitored and the final ΔTorque values are reported in Table 1 together with the sample composition.

Characterization/instrumentations

Size exclusion chromatography (SEC) analyses were performed in $CHCl_3$ (flux 0.3 mL min^{-1}) using an Agilent Technologies 1200 Series instrument equipped with two PLgel 5 μm MiniMIX-D columns and a refraction index detector. Monodisperse poly(styrene) samples (Agilent) were used as calibration standards.

X-ray diffraction (XRD) analysis was performed with a X'Pert PRO (PANalytical) powder diffractometer in the 1.5-15° 2θ range with a step size of 0.1050°, using Cu Kα radiation (1.541874 Å).

Transmission Electron Microscopy (TEM) was performed by using a Zeiss EM 900 microscope operating at an acceleration voltage of 80 kV. Ultrathin sections (about 50 nm thick) of compression-molded plaques were obtained by using a Leica EM FCS cryo-ultramicrotome equipped with a diamond knife.

Thermogravimetric analysis (TGA) was carried out using a Seiko EXSTAR 7200 TGA/DTA instrument. The analyses were carried out under nitrogen (200 mL min^{-1}) in the 30-700 °C range, at 10 °C min^{-1} scanning rate, on 5-10 mg samples. From the analysis of the thermograms was determined the onset degradation temperature (T_{onset}), which is the temperature corresponding to 5% mass loss, the rate and temperature values corresponding to the maximum degradation, and the final residue at 700 °C.

The Differential Scanning Calorimetry (DSC) analysis was performed using two different instruments: a differential scanning calorimeter Perkin-Elmer DSC7 calibrated using indium (T_m = 156.60 °C and ΔH_m = 28.38 J g^{-1}) and lead (T_m = 327.47 °C) as the reference standards. With this instrument the recrystallization temperature (T_{cc}), the melting temperature (T_m) and

the corresponding enthalpy values were determined. The samples were subjected to a first heating from 30 °C to 200 °C, to a cooling step from 200 °C to 30 °C and to a second heating scan from 30 °C to 200 °C at a speed of 10 °C min^{-1}. The determination of T_{cc}, T_m and the corresponding enthalpies were performed onto the second heating process. For the determination of the glass transition temperature (T_g) a differential scanning calorimeter DSC 7200 SEIKO EXSTAR was used. The instrument calibration was carried out by using indium and lead as the reference standards. For the determination of T_g the samples were subjected to a first process of heating from 30 °C to 180 °C, followed by a cooling process from 180 °C to -90 °C and a second process of heating from -90 °C at 90 °C which allowed us to assess the glass transition temperature. The rate of heating and cooling is 10 °C min^{-1}.

The Modulated Temperature Differential Scanning Calorimetry (MT-DSC) investigations have been performed with a Q100 calorimeter (TA instrument®). The instrument was calibrated for heat flow, temperature and baseline using standard T_{zero} technology. The nitrogen flow was 50 mL min^{-1} for all the experiments. The calibration of the temperature was carried out using standards like indium and zinc, and the calibration in energy was carried out using standard like indium. The calibration of the specific heat capacity was carried out using sapphire as a reference. Two different modes have been used: a heat-only mode (oscillation amplitude of 0.318 °C, oscillation period of 60 s and heating rate of 2 °C min^{-1} from 10 °C to 180 °C), which is advised to study the crystallization and the melting [36], and an heat-cool mode (oscillation amplitude of 2.5 °C, oscillation period of 100 s and heating rate of 1 °C min^{-1} from 10 °C to 70 °C) recommended to study the glass transition range and the molecular mobility in this region [36].

Results and discussion

Structural characterization

All the samples were prepared in the melt by mixing the polymer (PLA and eventually PLA and PBAT) with the organophilic clay (O-MMT) by using a Brabender mixer. During the runs the Torque values were monitored and after collecting the samples, the evolution of molecular weight was evaluated by SEC analysis (Table 1). Both the measurements are compelling to investigate the structural modification of the polymer matrix owing to the melt mixing of the filler. For comparison purpose PLA was treated in the Brabender by using the same experimental conditions used to provide the composites.

Table 1 Feed composition, ΔTorque values, SEC results

Materials	PBAT (% w)[1]	O-MMT (% w)[2]	ΔTorque[3]	$\overline{Mn}$ (D)	$\overline{Mw}$ (D)	I
PLA[4]	-	-	-	145000	217000	1.49
PLA_180[5]	-	-	1.03	160000	210000	1.31
PLA_O-MMT_1	-	1	1.00	118000	185000	1.56
PLA_O-MMT_2	-	2	1.16	116000	189000	1.62
PLA_PBAT_O-MMT_1	1	1	1.28	125000	194000	1.55
PLA_PBAT_O-MMT_2	2	2	1.24	144000	199000	1.38

[1] percentage by weight of PBAT with respect to the amount of PLA fed in the Brabender.
[2] percentage by weight of the introduced inorganic fraction (by considering that this is about 64% w/w of the O-MMT) with respect to the amount of PLA fed in the Brabender mixer
[3] ΔTorque = Initial Torque value (after melting of the polymer) – final Torque
[4] starting (not treated) PLA
[5] PLA treated in the Brabender at 180 °C

In general, the Torque variation between the beginning (after melting of the matrix) and the end of the mixing run appeared to be rather low, suggesting that the presence of the inorganic filler and the copolymer compatibilizer did not modify significantly the viscosity of the polymer matrix. Rather, it was observed a slight increase of ΔTorque by using both clay and PBAT (PLA_PBAT_O-MMT_1, PLA_PBAT_O-MMT_2). This evidence accounted the data of number average molecular weight (Mn) and weight average molecular weight (Mw). The heat treatment of the PLA at 180 °C did not substantially modify the molecular weight: only a slight increase of Mn can be noticed. The pretreatment of the polymer, which provides the heating at 110 °C for 12 hours under vacuum, seemed to ensure the removal of traces of water generally promoting the degradation processes of PLA at high temperature. However, the addition of the inorganic filler caused a decrease of the molecular weight (Mn) probably due to degradation effects attributable to hydrolysis caused by the presence of small amounts of water commonly present in inorganic fillers and/or functionalities characteristic of clay surfaces [37] [38], even if this reduction did not appear to depend on the quantity of the filler. Instead, the presence of PBAT limited the degradation effects and both the samples containing the compatibilizer showed significantly higher Mn with respect the corresponding sample provided without PBAT (PLA_PBAT_O-MMT_1 vs PLA_O-MMT_1 and PLA_PBAT_O-MMT_2 vs PLA_O-MMT_2). This result, which is depending on the amount of PBAT, and in agreement with the apparent viscosity behavior (ΔTorque) suggested that

PBAT chains can act at the interface preventing an intimate contact between the PLA and the clay surface.

Morphological features

X-ray diffractograms of the composite samples were compared with that of O-MMT (Figure 1). The characteristic *(001)* Bragg reflex of O-MMT shifted to lower reflection angles or disappeared which is in accordance with hybrid materials having intercalated or exfoliated morphologies. The data of the reflection angles and the relative basal distance reported in inset Table in Figure 1, clearly showed that for all the samples, with the exception of the sample PLA_O-MMT_1, there is an increase of the interlayer distance that does not seem to be affected by the amount of inorganic filler added to the matrix nor by the presence of the compatibilizer. Instead, in the case of the sample PLA_O-MMT_1, containing 1%w of the clay, no diffraction peak, attributed to the inorganic filler itself, could be observed; this experimental results might be indicative for a fully exfoliated morphology. It should be emphasized however that the systems examined cannot be classified as intercalated or exfoliated on the basis of the analysis of single diffraction signals. The hybrid material is best described as system where peculiar hybrid morphology statistically prevailed compared to the other without being representative for the whole sample; the structure was, in fact, not perfectly homogeneous, as illustrated by the analysis TEM. The "broadening" of the peak at lower angle particularly for samples PLA_PBAT_O-MMT_1 and PLA_PBAT_O-MMT_2 can be related both to a disorder of the sample in which clearly the platelets were not all perfectly aligned, or to a statistical distribution of interplanar distances, which can be determined, in average terms, by taking the 2θ angle corresponding to peak maximum as a reference.

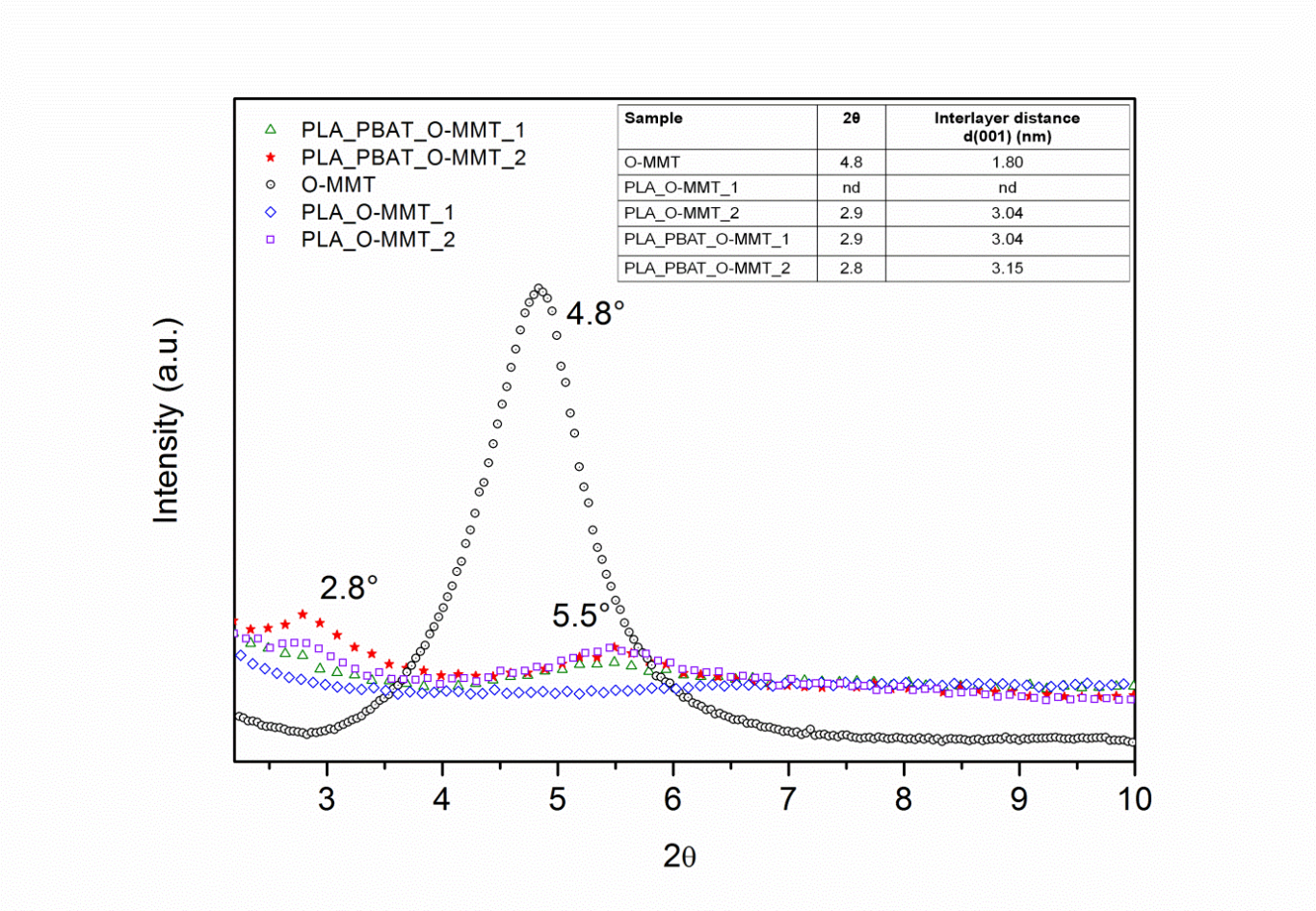

Sample	2θ	Interlayer distance d(001) (nm)
O-MMT	4.8	1.80
PLA_O-MMT_1	nd	nd
PLA_O-MMT_2	2.9	3.04
PLA_PBAT_O-MMT_1	2.9	3.04
PLA_PBAT_O-MMT_2	2.8	3.15

Figure 1 XRD patterns of composites and pristine O-MMT and evaluation of the interlayer distance based on Bragg's law

Accordingly, the composite PLA_PBAT_O-MMT_2 showed a shift of diffraction peak toward lower angles of 2θ = 2.8° (*d(001)* = 3.15 nm) thus being the sample having the highest interlayer distance. Moreover, in the composites with the higher filler contents it was evident a diffraction peak at 2θ = 5.5°, which is higher than the diffraction peak of O-MMT. This evidence can be justified [39][40][41] on the basis of mutual distribution of polymer phases and nanofiller lamellae, that gives an intercalated-flocculated morphology. In this case the ordered tactoids, generated upon intercalation of polymer chains in between the lamellae of O-MMT (intercalated morphology), can be interconnected through a strong interaction between the OH-groups on the polymer chain end and the surface of inorganic substrates giving a micro- and macro-aggregates As a result, an intercalated-flocculated morphology was obtained.

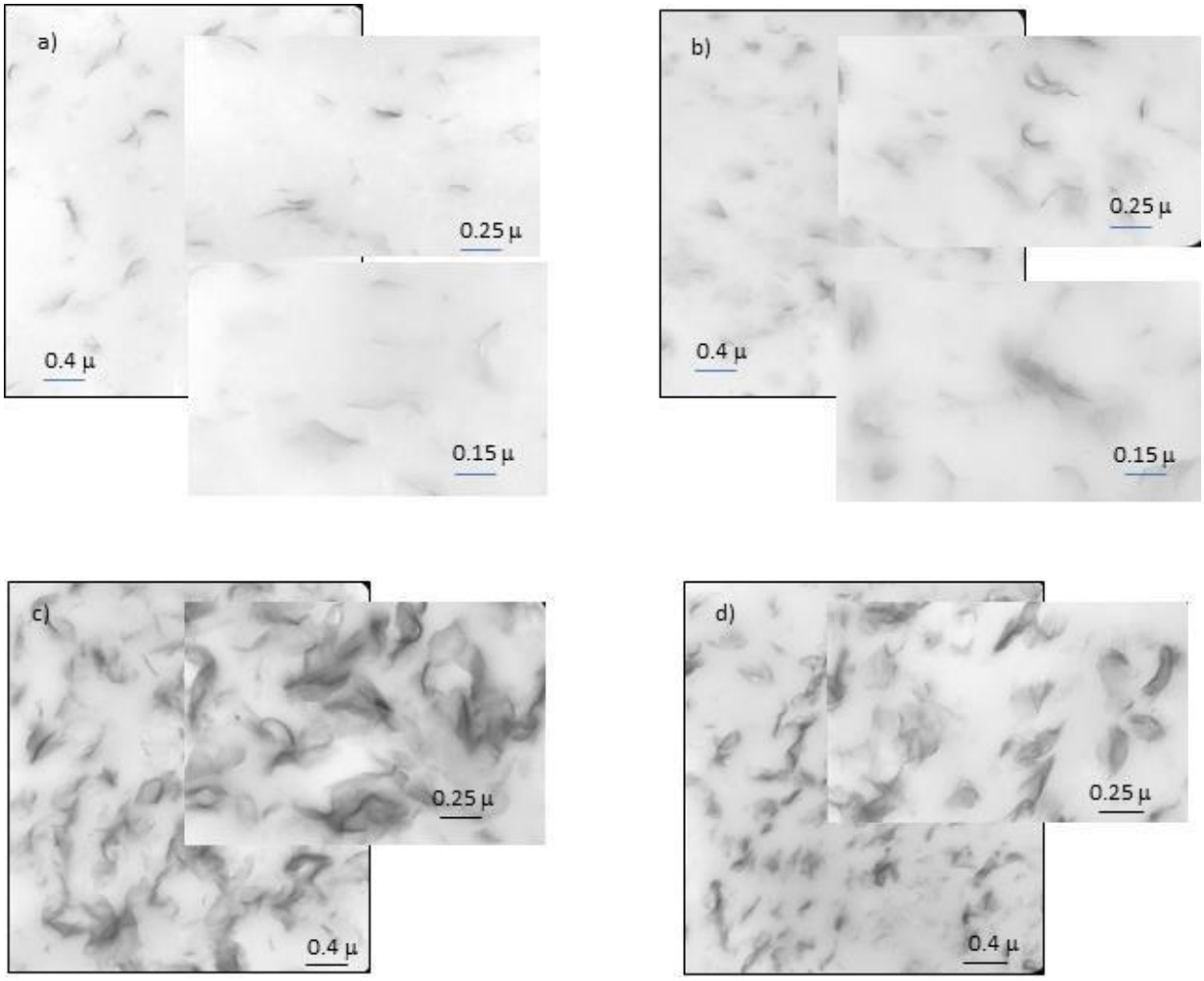

Figure 2 TEM micrographs of a) PLA_O-MMT_1; b) PLA_PBAT_O-MMT_1; c) PLA_O-MMT_2; d) PLA_PBAT_O-MMT_2

TEM micrographs (Figure 2) showed local morphologies of the different samples composed of single platelets; stacks (several stacked platelets, as in the pristine clay) and tactoids (stack agglomerates). All the samples showed a good dispersion of the platelets depending on the content of the filler, with more aggregates in samples with higher amount of clay without any apparent significant effect of the compatibilizer. A careful inspection at higher magnification showed a more homogeneous O-MMT dispersion in PLA_O-MMT_1 sample with respect to PLA_PBAT_O-MMT_1; a lot of single lamellae well-dispersed and completely disordered (not oriented) indicated a mainly exfoliated morphology. In both the samples with high content of clay, several intercalated stacks can be observed, indicating a substantially intercalated morphology. However, the presence of interconnected aggregates with different

dimensions (lower in the case of sample prepared by using PBAT) justifies the results collected by XRD assessing the morphology as intercalated-flocculated.

Thermal stability

The thermal degradation and the stability of PLA and nanocomposites were studied by thermogravimetric analysis (TGA) (experimental curves not shown here). The pure polymer processed at 180°C showed a single degradative step in a narrow interval of temperature (320-380 °C). Peak temperature (T_{max} i.e the temperature at maximum reaction rate) was placed at 366.6 °C. At 500 °C the char residue was about 0.3% w/w. All the nanocomposites showed a very similar behaviour: a unique stage of decomposition characterized by high peak temperature (in the same range of pure polymer), confirming that not significant structural variations occurred during the mixing with the nanostructured fillers (Table 2). A decrease in the decomposition onset temperature (T_{onset} i.e temperature at which the 5 % of initial mass is lost reflecting the stability features of the samples at early degradation stage) was observed for the sample containing 1% w/w of MMT. This experimental result might be attributed to the slight decrease of molecular weight leading to a more instable material. In addition the well-dispersed morphology of this sample granted an intimate contact between the polymer chain and the filler surface whose moisture (and residual adsorbed water) can affect the stability of the matrix [42]. By using the PBAT the thermal stability of PLA was totally restored, even at lower content of MMT, confirming its role as polymer coupling agent. The residual content of composites reflected the feed composition with really good agreement.

Table 2: Degradation temperatures and content of residual fractions under nitrogen

Materials	T_{onset} [1] (°C)	T_{max} [2] (°C)	Residue[3] (% wt)
PLA_180	330.0	366.6	0.31
PLA_O-MMT_1	326.0	366.6	1.40
PLA_O-MMT_2	336.0	367.3	3.45
PLA_PBAT_O-MMT_1	336.4	367.0	1.50
PLA_PBAT_O-MMT_2	336.5	367.8	3.22

[1] temperature corresponding to 5% of weight loss
[2] temperature of peak of DTGA curves
[3] residual fraction after complete decomposition (evaluated at 700 °C)

Preliminary study by classical DSC and XRD analyses

All the samples were characterized by DSC analysis first by using standard conditions of temperature scans (experimental curves not shown here). The data of the second heating scan were collected (Table 3). Since the absolute values of ΔH_{cc} and ΔH_m are almost identical, regardless of the samples they can be considered completely amorphous before DSC measurements. In all polymers with additives, a 1 °C decrease of the T_g value is recorded. This may be expected due to the effect of both the surfactant ammonium salt modifying the clay, (which effect is widely described in the literature for similar samples [43]), and the presence of PBAT. This polyester, really compatible with the PLA only in small quantities [44][45], has a T_g significantly lower than that of the PLA (around -45 °C), a value that may generate a further decrease in the T_g of the PLA/PBAT matrix composites. However, no correlation is found here between the weight percentage of additives and the glass transition temperature. Moreover the T_g variation is too low for a classical DSC analysis to be definitive about its significance. The decrease of the crystallization temperature along with the increase of the enthalpy of cold-crystallization, observed in particular for PLA_O-MMT_2, is attributable to a nucleating effect as the platelets facilitate the reorganization of the chains to assume a tidy structure, accelerating the crystallization process during the DSC run. This effect is inclusion size dependent: the greater the dispersion (sample PLA_O-MMT_1) the lower the nucleating effect.

Table 3 Thermal transition values and associated enthalpies

Materials	T_g[1] (°C)	T_{cc}[2] (°C)	T_m[3] (°C)	ΔH_{cc}[4] (J/g)	ΔH_m[5] (J/g)
PLA_180	58	129	154	-13	12
PLA_O-MMT_1	57	127	154	-16	16
PLA_O-MMT_2	57	123	151	-21	24
PLA_PBAT_O-MMT_1	57	127	152	-22	21
PLA_PBAT_O-MMT_2	57	128	153	-20	21

[1] glass transition temperature as determined in the second heating
[2] cold crystallization temperature
[3] melt temperature
[4] enthalpy of cold-crystallization
[5] enthalpy of melting

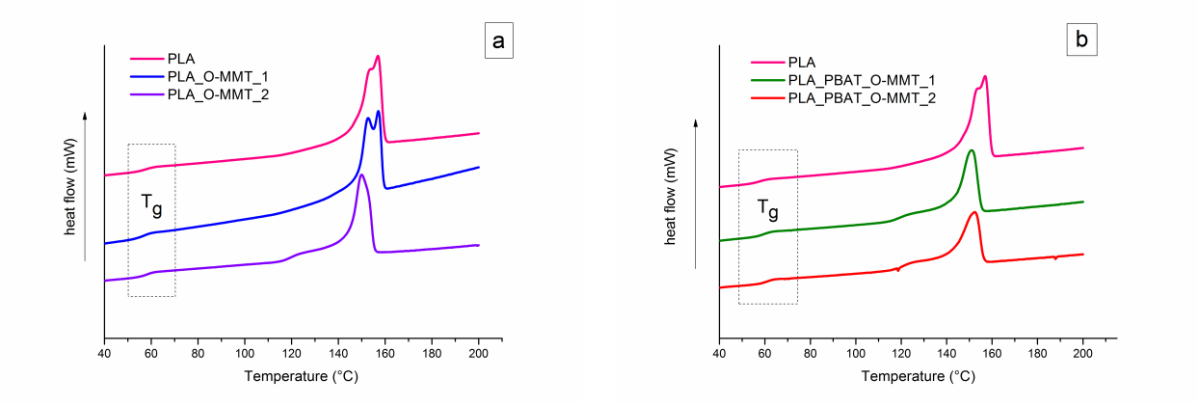

Figure 3 Thermograms corresponding to the heating of a) PLA samples with increasing content of filler b) and PLA samples with increasing content of filler and compatibilizer, after annealing at 110 °C for 18 hours.

In view of the fact that the recrystallization process is a phenomenon which depends on time, or on the rate of cooling and heating, DSC measurements were carried out on samples subjected to rapid cooling ("quenching") followed by annealing at 110 °C for 18 hours. The data obtained from the heating curve (Figure 3) of these samples, acquired at a rate of 10 °C min^{-1} are shown in Table 4. For all the analysed samples it was observed the disappearance of the re-crystallization peak (cold crystallization) confirming the complete annealing. The transition from amorphous polymer to the crystalline polymer was also confirmed by XRD analysis carried out before and after annealing: just after 2 hours of annealing at 110 °C, the diffraction peaks characteristic of the PLA (at angles 2θ : 14.3°, 16.7°, 19.3° and 22.3°) appeared with an intensity varying for longer annealing times (experimental curves not shown here). The glass transition temperature was visible without the characteristic enthalpy of relaxation, and with an associated value of specific heat (ΔCp) significantly lower than those observed for the samples analysed after "quenching" without annealing (from about 0.53 J g^{-1} $°C^{-1}$ to about 0.26 J g^{-1} $°C^{-1}$). Both the effects are characteristic of an increase of the crystalline fraction of the polymer. The accurate estimation of this crystalline fraction from calorimetric measurements requires to exactly know the enthalpy of melting (ΔH_{m0}) of 100% crystalline PLLA. Since this determination is still the focus of many recent studies [46] and has not for the moment given birth to a consensus, the usual value ΔH_{m0} = 93 J g^{-1} [47] has been chosen for the calculation of the degree of crystallinity. The enhancement of T_g values after annealing was, in first hypothesis, associated exclusively to the increase of the rigid amorphous fraction (RAF), resulting in the higher crystallinity. After an inspection, it appeared evident, however, that the values of T_g and crystallinity do not agree, and the sample with the higher value of crystallinity does not match the highest T_g. In particular, samples

containing PBAT with lower degree of crystallinity showed the highest values of T_g. The decrease of the enthalpy values for PLA-based composites with micro- and nano-fillers subjected to annealing was partially highlighted in the literature [40] and associated with morphological effects: an important surface area of interactions filler/polymer could on one side express in a reduced mobility of the chains interacting with the charge (increase of T_g) [48], on the other hand, especially in the presence of a high fraction of polymer intercalated-flocculated as in the case of the samples containing the PBAT, prevent the complete recrystallization (reduction of the crystallinity degree).

Table 4 Thermal transition values and associated enthalpy after annealing at 110 °C for 18 hours

Materials	T_g [1] (°C)	T_m [2] (°C)	ΔH_m [3] (J/g)	X_c [4] (%)
PLA_180	58	157	44	47
PLA_O-MMT_1	57	153/157	45	48
PLA_O-MMT_2	58	150	36	38
PLA_PBAT_O-MMT_1	59	151	37	39
PLA_PBAT_O-MMT_2	61	152	34	35

[1] glass transition temperature
[2] melting temperature
[3] enthalpy of melting
[4] degree of crystallinity determined from $X_c = \Delta H_m/\Delta H_{m0}*100$ by considering $\Delta H_{m0} = 93$ J g^{-1} as the enthalpy value of PLLA 100% crystalline [47]

In view of the fact that all the samples were undergone the same heat treatment, it was interesting to observe that the shape and the temperature of the melting peak was significantly different comparing the various composites. The PLA after annealing showed a shoulder in the melting peak at about 152 °C while the sample PLA_O-MMT_1 had an evident double melting peak (at 152.9 °C and 157.1 °C). The samples PLA_O-MMT_2, PLA_PBAT_O-MMT_1 and PLA_PBAT_O-MMT_2 showed a broad melting peak "pulled aside" to values of temperatures around 152 °C or less. Also, these three samples showed another endothermic peak (much enlarged) between 120 and 140 °C. Zhang and co-authors [49] demonstrated for the PLA the existence of two crystalline forms of type α: in particular, they highlighted the presence of a "disordered" form (α') with regard to the conformation and modes of "packing" of the chains, characterized by a lower melting temperature [33]. When the samples were annealed at 110°C ≤ T annealing ≤ 120°C, the PLA recrystallized in this T range showed

crystalline domains in both co-existing forms α and α' with prevalence of the form α', resulting in a complex melting peak. Because the transition of the form α' (considered metastable) to the form α (more ordered) depends only on the temperature and annealing time, the differences observed for the composites, all treated in the same experimental conditions, could be attributed to the presence of the clay and its dispersion degree in the polymer matrix. The clay and the PBAT then "disturb" the crystallization process not only by reducing the crystallinity degree of the polymer, but also favouring the formation of crystals more disordered which melt at lower temperatures. Whereas some authors suggest a correlation between the endothermic peak below melting and the relaxation enthalpy of the RAF [50], others would associate the peak pulled aside between 120°C and 140°C in the samples PLA_O-MMT_2, PLA_PBAT_O-MMT_1 PLA_PBAT_O-MMT_2 to a transition α'-α or transitions α'-α' with different order and magnitude of spherulites [49][51].

To further investigate this aspect, and better assess the effects of morphology, namely the dispersion of the filler, onto the shape of the spherulites, a comparison between the XRD spectra of the sample PLA and its composites after annealing was carried out. On the basis of the attributions reported in the literature for the α form we noticed that the position of the peaks *(200/100)* and *(203)* was shifted towards lower angles 2θ for samples containing the O-MMT. It was reported that in particular the profile of the reflection *(203)* can be resolved into two components originating from the forms and α and α', which is in accordance with the trend shown in Figure 4, and the behaviour reported by Zhang [49] as a function of the annealing temperature. From the Scherrer equation applied to reflection *(203)* we can roughly estimate the thickness of crystalline lamellae *D* shown in inset Table of Figure 4 for selected composite samples:

$$D = \frac{K\,\lambda}{b\,cos\theta} \tag{1}$$

Where, D is the thickness of a crystalline lamella in nm, K a dimensionless form factor (K = 0.94), b the half band height of the diffraction peak, θ is the Bragg angle. From a comparison of these latter X-ray diffraction data with data reported in the literature [49] it was clear that these values are consistent with the presence of a mixed phase where the two forms α and α' coexist. Although the data collected essentially confirm that the annealing at 110 °C gave rise to samples in which the two phases coexist with prevalence of form α', it was clear that the

sample PLA_O-MMT_1 is characterized by a greater disordered crystalline phase. This sample has also the largest size of the crystalline lamellae indicating an increase in the regularity of the structure of the form α' although the degree of order of the form α is certainly higher. This effect could be associated, in the first hypothesis, to the greatest degree of dispersion, or to the higher content of exfoliated fraction that, as widely reported in the literature [52] promotes the growth of spherulites of larger dimensions than in the intercalated morphology where the chains are subjected to confinement effects. The comparison of the samples with the lowest percentage of charge (1% w/w) with or without PBAT showed that the latter does not influence the formation of different crystalline phases as the profiles of reflections *(200/110)* and *(203)* do not change, confirming the complete miscibility of polymer in the compositions used. These results show that the dispersion at the nanometer level of the filler significantly affected not only the thermal properties of the bulk, but also the formation and the coexistence of the two crystalline phases, so far shown only as an effect of different heat treatment.

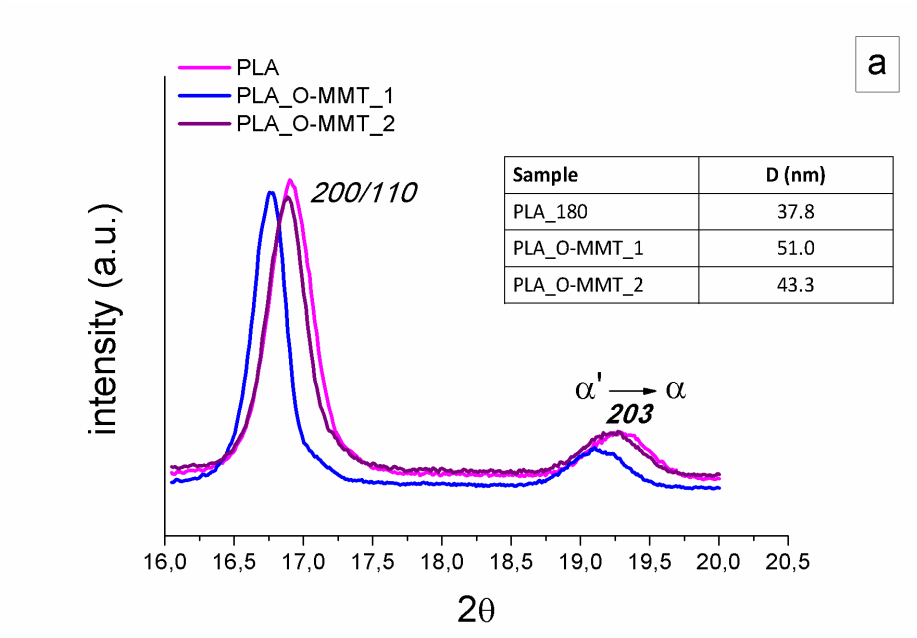

Sample	D (nm)
PLA_180	37.8
PLA_O-MMT_1	51.0
PLA_O-MMT_2	43.3

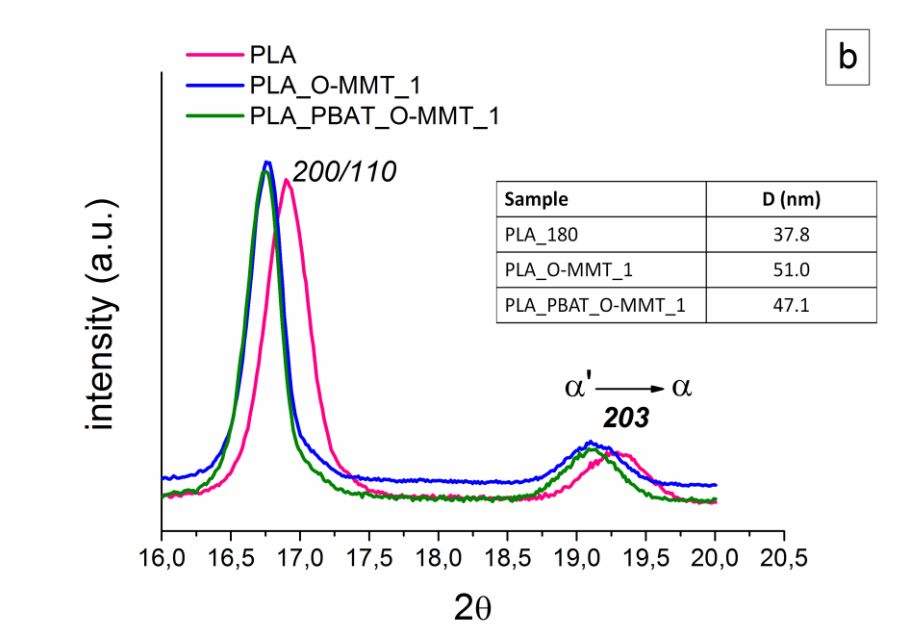

Sample	D (nm)
PLA_180	37.8
PLA_O-MMT_1	51.0
PLA_PBAT_O-MMT_1	47.1

Figure 4 XRD spectra in the 2θ range from 16.0° to 20.5° of a) PLA_180 and its composites with 1%w and 2%w of O-MMT and b) PLA_180 and its composites with 1% w of O-MMT in presence and absence of PBAT. D is the thickness of a crystalline lamella as estimated by Scherrer equation (tables in inset).

Annealings studied by MT-DSC investigations

In order to distinguish the influence of the composition on the crystallisation behaviour, we performed two different annealings: one at 80 °C (generating only the α' crystalline form) and one at 130 °C (generating only the α crystalline form) during 8h after quenching from the melt. To optimize the accuracy, the thermal characterization has been performed by MT-DSC with a heat-only mode.

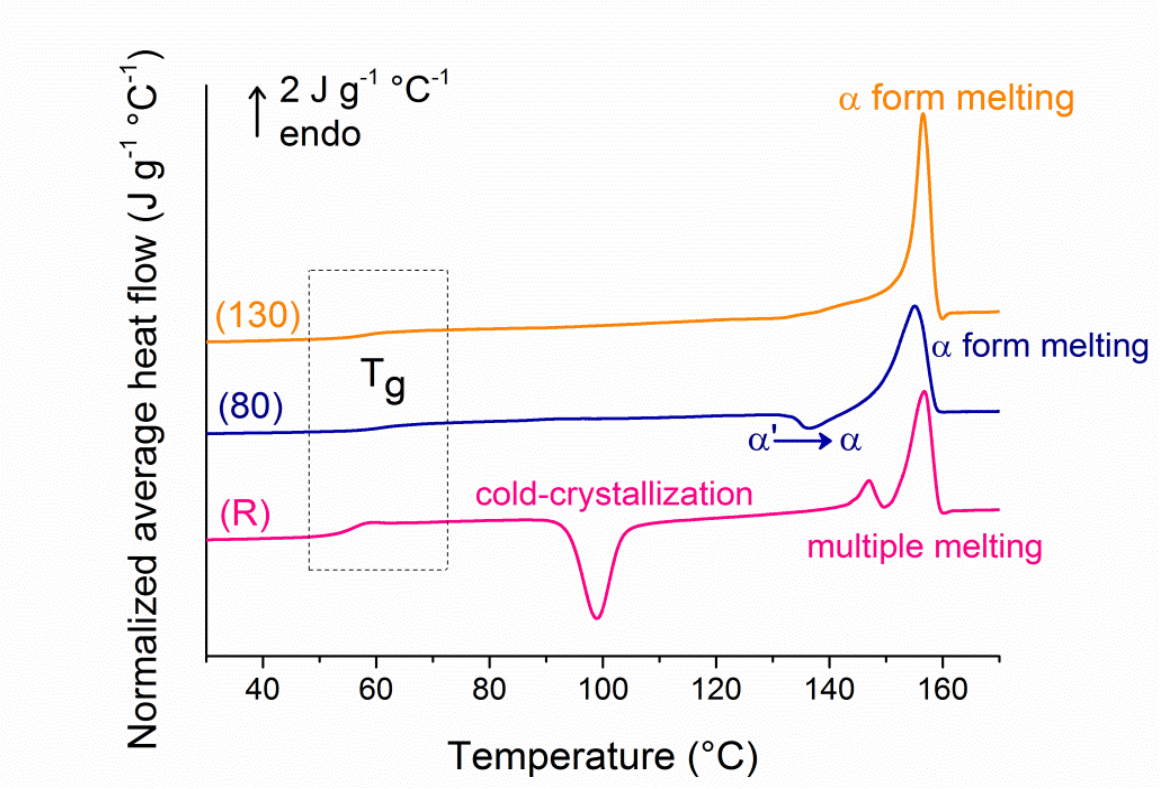

Figure 5 MT-DSC investigations: Evolution of the normalized average heat flow as a function of temperature for PLA_180 after quenching from the melt (R), annealing at 80 °C during 8h (80), and annealing at 130 °C during 8h (130).

Figure 5 shows the evolution of the normalized average heat flow as a function of temperature for PLA_180 after quenching from the melt as a reference (R), annealing at 80 °C during 8h (80), and annealing at 130 °C during 8h (130). The quenched sample (R) shows a classical behaviour for PLA with three thermal phenomena [53]: an endothermic step around 55 °C corresponding to the glass transition, a cold crystallization around 100 °C leading to the concomitant crystallization under both α and α' forms, and finally a complex melting double peak around 150 °C which existence has widely been reported in literature [54][55][56]. The lowest temperature endothermic peak is generally attributed to the perfect crystal melting, associated with the defective crystal transformation into more perfect crystals as melting and recrystallization of unstable crystals take place almost simultaneously [57]. The highest temperature endothermic peak corresponds to the perfect crystal melting, arisen from their fusion-recrystallization or from the defective crystal transformation. The sample annealed at 80 °C during 8h (b) shows a lower endothermic step at the glass transition than the rejuvenated sample (in agreement to the presence of crystalline phase), an exothermic peak corresponding to the reorganization of the α' crystalline form to α one [49] and an

endothermic peak related to the α form melting. Di Lorenzo has shown that the crystallization at low temperatures (T_c < 120 °C) leads to the achievement of low crystallinity degree values, with formation of small and/or defective crystals, having a large tendency to reorganize into more stable structures during the heating scan [54]. The sample annealed at 130°C during 8h (c) shows a similar endothermic step at the glass transition than the sample annealed at 80°C, and only an endothermic peak at higher temperature related to the α form melting. Classically the two annealings generate different microstructures [53]. Although the normalized average heat flow step and therefore the content of amorphous phase relaxing at the glass transition is quite the same for a given sample, the crystallization under the α form (130) leads to higher crystallinity degree, whereas the crystallization under the α' form (80) leads to lower crystallinity degree and higher RAF content (Table 5). This behaviour has been explained in literature by the lack of chain mobility at low crystallization temperatures that hinders the reorganization of polymeric segments in crystals and induces many chain segments subjected to geometrical restrictions [58]. All the thermal characteristics are given in Table 5. Figure 6a gives the evolution of the normalized average heat flow as a function of temperature for filled PLA with 1% or 2% w/w. By comparison with the unfilled PLA (Figure 5), this exhibits notable similarities. Nevertheless the filler content sensitively influences the thermal behaviour, especially the glass transition temperature for quenched samples as clearly shown in the inset (Figure 6a): The glass transition temperature is significantly shifted at higher temperature for PLA_O-MMT_1 in comparison to PLA_180 but also in comparison to PLA_O-MMT_2. As widely reported in the literature [59][60][61][62][63], this shift of T_g can be correlated to the exfoliated morphology of this sample because of the strong interactions between PLA and O-MMT. We may note that this shift was only identifiable thanks to the MT-DSC measurements that allow investigating the glass transition with high resolution.

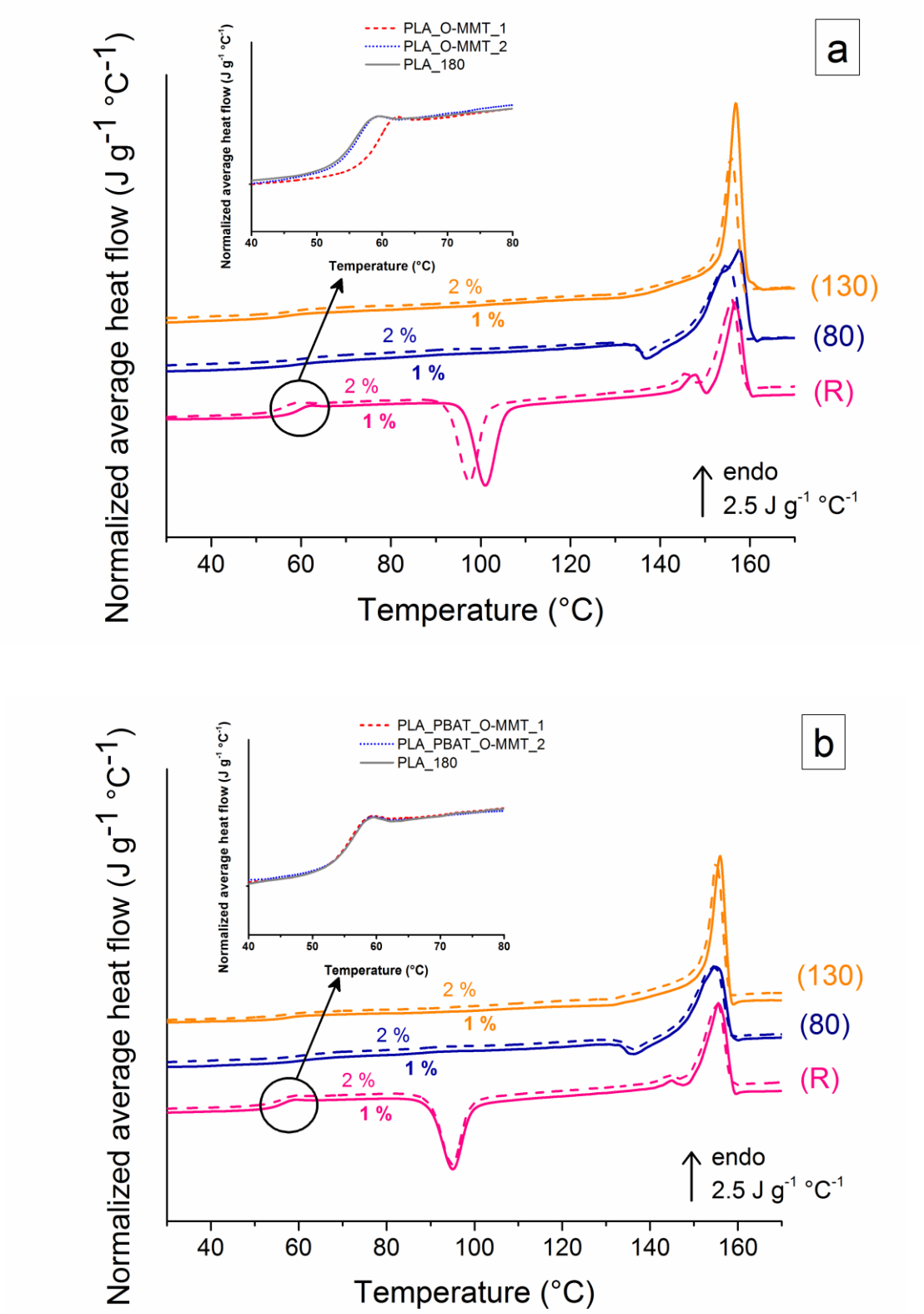

Figure 6 MT-DSC investigations: Evolution of the normalized average heat flow as a function of temperature for (a) filled PLA and (b) filled and compatibilized PLA (with 1% or 2% W/W) after quenching from the melt (R), annealing at 80°C during 8h (80), and annealing at 130°C during 8h (130). The insets correspond to a zoom in the glass transition region for quenched samples.

Table 5 Structural and thermal parameters from MT-DSC Heat Only investigations.

Materials	Treatment	$T_{g\ mid}$ [1] (°C)	ΔC_p [2] ($Jg^{-1}°C^{-1}$)	ΔH_{cc} [3] ($Jg^{-1}°C^{-1}$)	ΔH_m [4] ($Jg^{-1}°C^{-1}$)	X_{ma} [5] (%)	X_c [6] (%)	X_{ra} [7] (%)
PLA_180	R	54,9	0,53	29	29	100	0	0
	80	61,1	0,26	3	30	49	29	22
	130	58,3	0,24	no cc	40	45	43	12
PLA_O-MMT_1	R	58,3	0,55	36	37	100	0	0
	80	61,4	0,21	4	38	38	37	25
	130	59,5	0,24	no cc	49	44	53	3
PLA_O-MMT_2	R	55,1	0,51	29	31	100	0	0
	80	59,7	0,2	3	31	39	30	31
	130	58,8	0,21	no cc	40	41	44	15
PLA_PBAT_O-MMT_1	R	55,2	0,47	29	33	100	0	0
	80	61,5	0,22	3	31	47	31	22
	130	57,4	0,22	no cc	41	47	44	9
PLA_PBAT_O-MMT_2	R	55	0,49	29	30	100	0	0
	80	60,8	0,24	3	30	49	31	20
	130	57,4	0,25	no cc	39	51	43	6

[1] glass transition temperature taken at middle point
[2] variations of the specific heat at T_g
[3] enthalpy of cold-crystallization
[4] enthalpy of melting
[5] mobile amorphous fraction calculated from $X_{ma} = \Delta C_p/\Delta C_{p0}$ by considering ΔC_{p0} as the value for the rejuvenated sample.
[6] degree of crystallinity determined from $X_c = \Delta H_m/\Delta H_{m0}*100$ by considering $\Delta H_{m0} = 93\ Jg^{-1}$ as the enthalpy value of PLLA 100% crystalline [47].
[7] rigid amorphous fraction calculated from $X_{ra} = 100 - (X_{ma} + X_c)$

Independently on the annealing procedure, we observe that the resulting enthalpy of melting and therefore the degree of crystallinity are significantly higher for PLA_O-MMT_1 in comparison to PLA_180 but also in comparison to PLA_O-MMT_2. It is reasonable to assume that the initial exfoliated morphologies favour the growth of the crystalline phase during the annealing. We also observe that for both annealing procedures, the melting peak for PLA_O-MMT_1 is shifted towards higher temperatures. This result is consistent with the

XRD analysis, suggesting the generation of higher dimension spherulites. PLA_O-MMT_1 annealed at 80°C also exhibits a broader α' to α reorganization exothermic peak and a broader melting peak that might even look bimodal. Assuming this, one can observe that the low temperature contribution is recorded in the same temperature range than the melting peak of PLA_O-MMT_2 when the high temperature contribution is recorded at higher temperatures. We suppose that each contribution is characteristic of a degree of exfoliation. The low temperature contribution would be associated to the melting of crystals formed in areas where the morphology is intermediate between exfoliated and intercalated. On the other hand the high temperature contribution would be associated to the melting of crystals formed in areas where the morphology is wholly exfoliated. Obviously this fully exfoliated morphology only exists in PLA_O-MMT_1. Figure 6b gives the evolution of the normalized average heat flow as a function of temperature for filled and compatibilized PLA (1% or 2% w/w). All the thermal characteristics are given in Table 5. Independently on the PBAT content, the profile of the curves is strongly similar. Therefore, contrary to filled non compatibilized PLA, the enthalpies of cold-crystallization and melting as well as the degree of each phase are only dependent on the chosen annealing procedure. For the quenched materials (R), the glass transition and both enthalpies of cold-crystallization and melting are identical to those of PLA_180 and PLA_O-MMT_2 but lower compared to the values recorded for PLA_O-MMT_1. Obviously in PLA_PBAT_O-MMT_1, the presence of PBAT acting at the interface between the PLA and the O-MMT erases the effects induced by the exfoliated morphology on the glass transition, the cold-crystallization and the melting. These results are consistent with the improvement of the thermal stability observed in TGA which evidences the role of PBAT as coupling agent. On the other hand no modification of the thermal behaviour related to the presence of PBAT is recorded for PLA_PBAT_O-MMT_2. We assume that the positioning of PBAT at the interface between O-MMT and PLA is of lesser importance when the content of O-MMT is equal to 2% w/w, due to the structural dominance of the intercalated laminates that do not exhibit the same level of interaction with PLA than exfoliated nanofillers. When annealed at 80°C or 130°C, PLA_PBAT_O-MMT_1 and PLA_PBAT_O-MMT_2 exhibit the same thermal behaviour than PLA_180 which does not confirm the assumption that the PBAT will cause the decrease of the crystallinity degree. The annealing procedure leads to lower enthalpy of melting and crystallinity degree for PLA_PBAT_O-MMT_1 compared to PLA_O-MMT_1 in accordance with the positioning of PBAT at the matrix/filler interface that counteracts the role of the exfoliated morphology in

the crystal growth. It is also noteworthy that the degree of RAF generated during the annealing is low compared to filled non compatibilized nanocomposites and especially to PLA_O-MMT_2 where the structural hindrance brought by the intercalated clay layers is high. This might be related to the role of the compatibilizer that provides more mobility to the PLA chains in order to ensure a better decoupling between amorphous and crystalline phases during the annealing.

Molecular mobility of the amorphous phase studied by MT-DSC investigations

To investigate the molecular mobility in the amorphous phase, we performed MT-DSC by heating with a heat-cool mode in the glass transition range from 35 °C to 85 °C. Indeed, by this way, it is possible to estimate the cooperativity degree of the molecular movements occurring at the glass transition. To estimate the CRR size at the glass transition temperature, it is possible to use the Donth's model [10] based on calorimetric investigations from which the cooperativity degree noted N_α can be estimated with the equation (2):

$$N_\alpha = \frac{(1/C_p)_{Glass} - (1/C_p)_{Liquid}}{M_0(\delta T)^2} N_A \, k_B T_g^2 \qquad (2)$$

Where, T_g is the dynamic glass transition temperature correlated to the oscillation period chosen, k_B the Boltzmann constant, N_A the Avogadro's number, M_0 the molar mass of the monomeric unit and δT the temperature fluctuation in a CRR. From an experimental point of view, the way to extract all the quantities needed to calculate the cooperativity degree, i.e., T_g, ΔCp^{-1}, and δT, is described in details in reference [64]. As an example, the Figure 7 gives the evolution of the in-phase and out-of-phase components of the complex heat capacity as a function of temperature for PLA_O-MMT_1 after quenching from the melt as a reference (R), annealing at 80°C during 8h (80), and annealing at 130°C during 8h (130). Classically, the annealing processes induce a broadening of the glass transition step (increase of δT) that also appears with weak amplitude due to the lower amount of amorphous phase relaxing at the glass transition. It is assumed that in maximum crystallized PLA, whatever annealing procedures, the entire Mobile Amorphous Fraction (MAF) that undergoes the glass transition is trapped into spherulites [65]. This intra-spherulitic MAF has its own relaxation parameters that strongly differ from those of the amorphous matrix, i.e., higher T_g and δT, and lower cooperativity degree N_α. These differences have been related to the cumulated effect of pure geometrical confinement of the amorphous phase induced by the crystals and to the

incomplete decoupling between the amorphous and the crystalline phases leading first to the RAF development and second to the restriction of the chain mobility in the intra-spherulitic MAF. Compared to the annealing at 130 °C, the annealing at 80 °C leads to higher values of T_g and δT and to a lower value of N_α, suggesting that the MAF is more constrained.

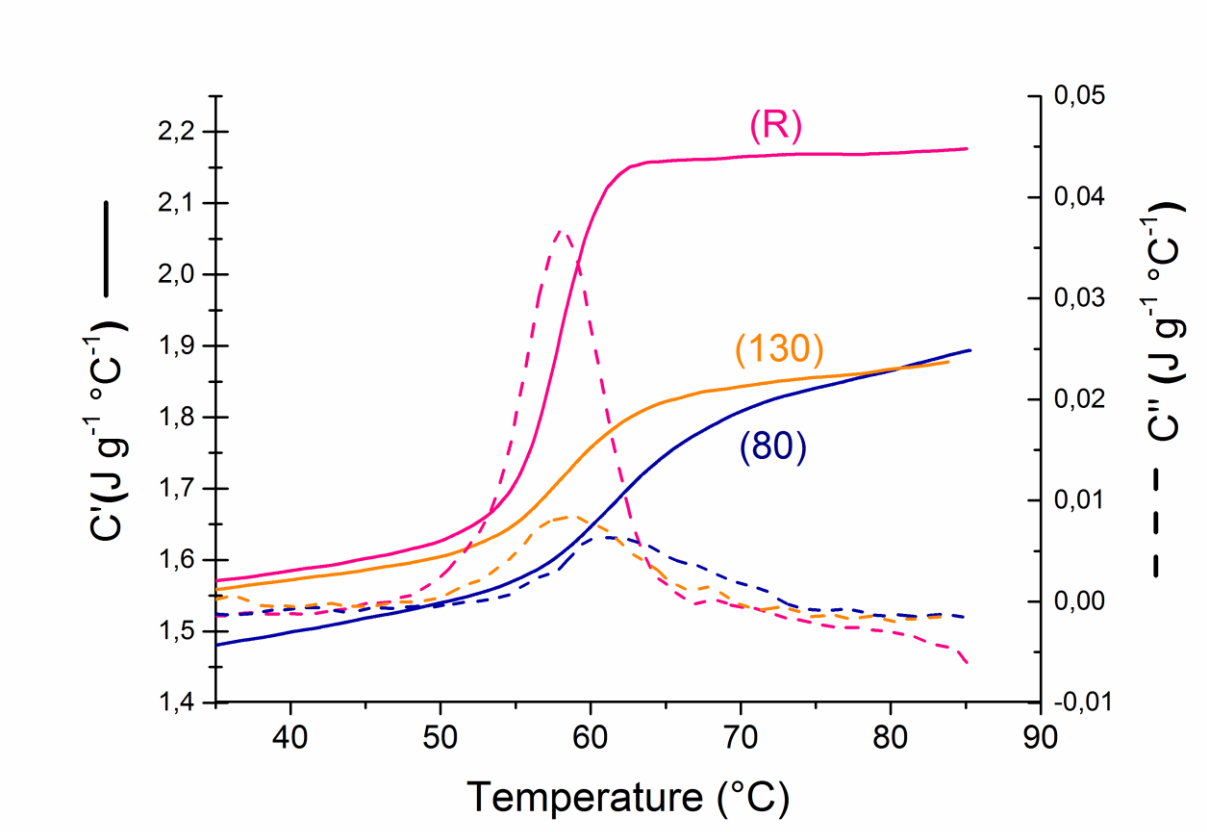

Figure 7 MT-DSC in-phase and out-of-phase components of the complex heat capacity as a function of temperature for PLA_O-MMT_1 after quenching from the melt (R), annealing at 80°C during 8h (80), and annealing at 130°C during 8h (130).

In Figure 8a, the values of N_α are presented for the quenched materials (R). Considering PLA_180 as reference, PLA_O-MMT_1 exhibits higher cooperativity. On the other hand, N_α decreases for PLA_O-MMT_2, PLA_PBAT_O-MMT_1 and PLA_PBAT_O-MMT_2. The role of the morphology on the cooperativity is schematized in Figure 8b following the structural representation of the cooperativity proposed in ref. [34]. In PLA_O-MMT_1, the cooperativity increase could be attributed to the interfacial interactions between the filler and the matrix. When adding PBAT, these interactions disappear because of the positioning of PBAT at the clay/matrix interface. Since O-MMT is homogenously dispersed in PLA matrix, the inter-chain bond breaking strongly decreases N_α. For PLA_O-MMT_2, the intercalated-flocculated structures that can interact together behave as pure steric hindrances, limiting the

CRR domain. Therefore the role of PBAT is more limited, as the cooperativity is not driven by interfacial interactions, so N_α does not evolve.

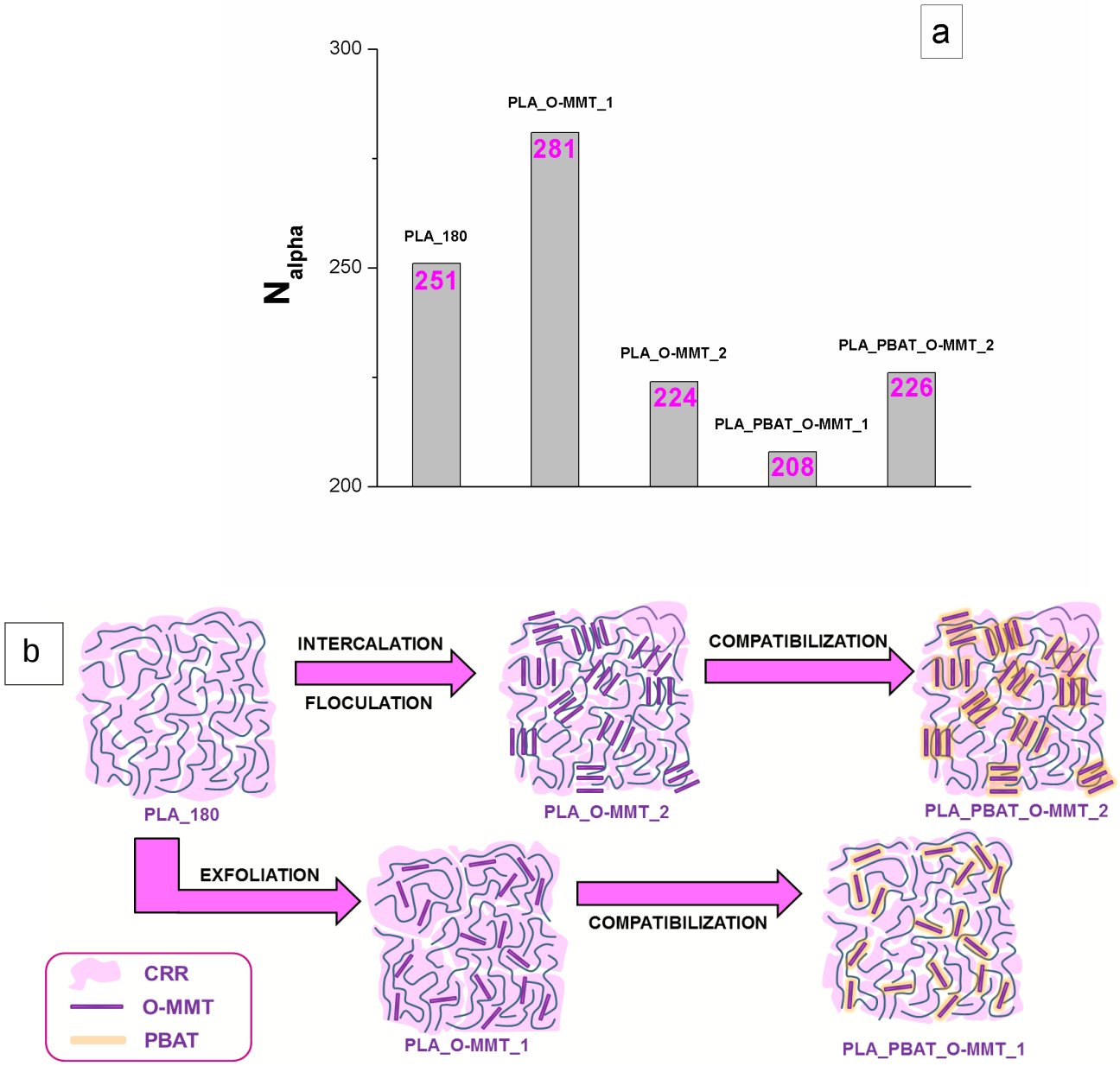

Figure 8 Morphological dependences of the cooperativity: (a) Cooperativity degree for quenched materials; (b) Structural schematization of the relation between cooperativity and morphology in quenched materials

To assess whether the morphology also influences the cooperativity post-crystallization, we report in Figure 9 the values of N_α for all materials. For α and α' crystallized materials, polarized optical microscopy pictures (POM) have been added. Quickly the surface of α' crystallized materials becomes fully covered by small size imperceptible spherulites which

maximum diameter is equal to 20 µm. On the other hand, after one hour and two hours of crystallization under the α form, the spherulites are clearly distinguishable and their maximum diameters reach 170 µm after two hours of crystallization. Obviously these annealed materials exhibit close cooperativity degrees compared to amorphous. Moreover, N_α seems to be mainly dependent on the nature of the annealing procedure. The annealing at 80 °C, generating α' crystalline form, leads to lower values of N_α. Compared to the annealing at 130 °C, this crystallization induces first the formation of significantly lower size spherulites as already observed by Pluta and Galeski [66] and also to a higher content of Rigid Amorphous Fraction, being both signatures of an imperfect crystallization. As a consequence, two main reasons may explain the higher impact that this annealing procedure has on cooperativity. The confinement of the MAF may be more important when it is trapped into α' crystals than into α crystals. This hypothesis is consistent with the Small-Angle X-Ray Scattering results from Tsuji et al. [67] who observe a decrease of the average amorphous layer thickness when decreasing the temperature of crystallization. One can also consider the relation between the temperature fluctuation and the environmental heterogeneity [68] likely brought by the high content of Rigid Amorphous Fraction which additionally restricts the chain motion in the MAF.

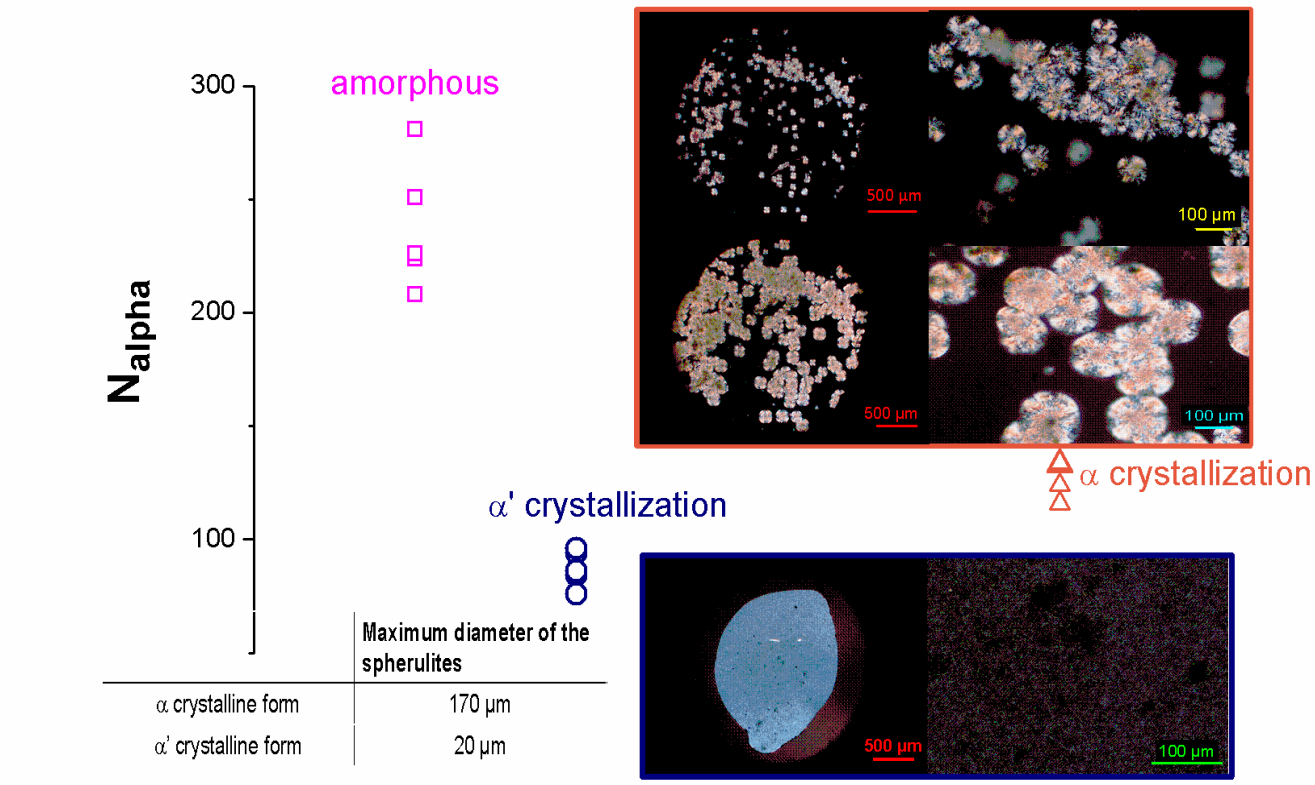

Figure 9: Cooperativity degree for quenched and annealed samples. For α crystallization, Polarized Optical Microscopy pictures correspond to 1 h (top) and 2 h (bottom) annealing of PLA_O-MMT_1. For α' crystallization, Polarized Optical Microscopy pictures correspond to 3 h annealing of PLA_O-MMT_1.

Conclusion

The cooperativity degree obtained from MT-DSC is a powerful complementary tool to X-Ray diffraction and microscopy when investigating the morphology of nanocomposites since it probes the physical interactions between the matrix and the filler. When the dominant morphology of the nanocomposite is exfoliated, the interfacial interactions between the matrix and the filler increase the cooperativity. On the other hand, intercalated morphology renders less effective the formation of physical bonds due to the confinement of the macromolecules in the galleries of fillers, decreasing hence the cooperativity degree. In this work it is shown that the investigation of the cooperativity degree is also important to characterize the efficiency of a coupling agent in providing PLA-based nanocomposites with suitable morphology. The localization of PBAT at the interface between the PLA and the O-MMT by breaking the matrix/filler physical bonds existing for the exfoliated morphologies brings about a strong decrease of cooperativity, whereas it has no influence when the cooperativity degree is already lowered by the confining effect of flocculated aggregates. While the interaction level at the PLA/O-MMT interface differently promotes the crystallization under the α and/or α' forms and the distribution of the rigid/mobile amorphous fractions, it has a low effect on the cooperativity degree in semi-crystalline nanocomposites. In that case the amorphous areas are strongly confined and part of the amorphous phase has restricted mobility due to the coupling between the amorphous and the crystalline phases. Therefore the cooperative nature of the molecular motions is too severely limited by the crystals and the RAF to observe any effect due to the morphology.

Acknowledgements

MIUR (PRIN 2008); Materiali nanoibridi a base biopoliesteri:miscelazione reattiva di sistemi organici e inorganici opportunamente modificati". contract grant number: 200898KCKY is acknowledged for partially funding the research

References

1. Chen K, Wilkie CA, Vyazovkin S (2007) Nanoconfinement revealed in degradation and relaxation studies of two structurally different polystyrene−clay systems. J Phys Chem B 111:12685–12692. doi: 10.1021/jp0759168
2. Leszczynska A, Pielichowski K (2008) Application of thermal analysis methods for characterization of polymer/montmorillonite nanocomposites. J Therm Anal Calorim 93:677–687. doi: 10.1007/s10973-008-9128-6
3. Couderc H, Saiter A, Grenet J, et al. (2011) Gradient of molecular dynamics at the glass transition of PETg–Montmorillonite nanocomposites. Phys B Condens Matter 406:2908–2913. doi: 10.1016/j.physb.2011.04.064
4. Greco A, Gennaro R, Rizzo M (2012) Glass transition and cooperative rearranging regions in amorphous thermoplastic nanocomposites. Polym Int 61:1326–1333. doi: 10.1002/pi.4212
5. Saiter A, Prevosto D, Passaglia E, et al. (2013) Cooperativity length scale in nanocomposites: Interfacial and confinement effects. Phys Rev E 88:042605. doi: 10.1103/PhysRevE.88.042605
6. Khan AN, Hayder A, Chaung WT, et al. (2015) Glass transition behavior of poly(trimethylene 2,6-naphthalate) in nanoclay confinement. Composites Polymer Science Series A 57:874–882. doi 10.1134/S0965545X15060127
7. Sharma M, Madras G, Bose S (2014) Cooperativity and structural relaxations in PVDF/PMMA blends in the presence of MWNTs: An assessment through SAXS and dielectric spectroscopy. Macromolecules 47:1392–1402. doi: 10.1021/ma4023718
8. Sharma M, Madras G, Bose S (2015) Unusual fragility and cooperativity in glass-forming and crystalline PVDF/PMMA blends in the presence of multiwall carbon nanotubes. Macromolecules 48:2740–2750. doi: 10.1021/acs.macromol.5b00418
9. Adam G, Gibbs JH (2004) On the temperature dependence of cooperative relaxation properties in glass-forming liquids. J Chem Phys 43:139–146. doi: 10.1063/1.1696442
10. Donth E (1982) The size of cooperatively rearranging regions at the glass transition. J Non-Cryst Solids 53:325–330. doi: 10.1016/0022-3093(82)90089-8
11. Hempel E, Hempel G, Hensel A, et al. (2000) Characteristic length of dynamic glass transition near Tg for a wide assortment of glass-forming substances. J Phys Chem B 104:2460–2466. doi: 10.1021/jp991153f
12. Casalini R, Fragiadakis D, Roland CM (2011) Relaxation dynamics of poly(methyl acrylate) at elevated pressure. Macromolecules 44:6928–6934. doi: 10.1021/ma200892f
13. Delpouve N, Vuillequez A, Saiter A, et al. (2012) Fragility and cooperativity concepts in hydrogen-bonded organic glasses. Phys B Condens Matter 407:3561–3565. doi: 10.1016/j.physb.2012.05.024
14. Furushima Y, Ishikiriyama K, Higashioji T (2013) The characteristic length of cooperative rearranging region for uniaxial drawn poly(ethylene terephthalate) films. Polymer 54:4078–4084. doi: 10.1016/j.polymer.2013.06.030
15. Arabeche K, Delbreilh L, Saiter J-M, et al. (2014) Fragility and molecular mobility in micro- and nano-layered PC/PMMA films. Polymer 55:1546–1551. doi: 10.1016/j.polymer.2014.02.006
16. Tran TA, Saïd S, Grohens Y (2005) Nanoscale characteristic length at the glass transition in confined syndiotactic poly(methyl methacrylate). Macromolecules 38:3867–3871. doi: 10.1021/ma0487296

17. Rijal B, Delbreilh L, Saiter A (2015) Dynamic heterogeneity and cooperative length scale at dynamic glass transition in glass forming liquids. Macromolecules 48:8219–8231. doi: 10.1021/acs.macromol.5b01152
18. Nakanishi M, Nozaki R (2011) Model of the cooperative rearranging region for polyhydric alcohols. Phys Rev E 84:011503. doi: 10.1103/PhysRevE.84.011503
19. Grigoras CV, Grigoras AG (2010) Nanoscale cooperativity on a series of statistical methacrylates copolymers with electron donor–acceptor pendant groups. J Therm Anal Calorim 103:661–668. doi: 10.1007/s10973-010-1019-y
20. Dobircau L, Delpouve N, Herbinet R, et al. (2015) Molecular mobility and physical ageing of plasticized poly(lactide). Polym Eng Sci 55:858–865. doi: 10.1002/pen.23952
21. Paluch M, Pawlus S, Grzybowski A, et al. (2011) Fragility versus activation volume: Insight into molecular dynamics of glass-forming hydrogen-bonded liquids. Phys Rev E 84:052501. doi: 10.1103/PhysRevE.84.052501
22. Bouthegourd E, Esposito A, Lourdin D, et al. (2013) Size of the cooperative rearranging regions vs. fragility in complex glassy systems: Influence of the structure and the molecular interactions. Physica B 425:83–89. doi:10.1016/j.physb.2013.05.029
23. Reddy MM, Vivekanandhan S, Misra M, et al. (2013) Biobased plastics and bionanocomposites: Current status and future opportunities. Prog Polym Sci 38:1653–1689. doi: 10.1016/j.progpolymsci.2013.05.006
24. Rhim JW, Park HM, Ha CS (2013) Bio-nanocomposites for food packaging applications. Prog Polym Sci 38:1629–1652. doi: 10.1016/j.progpolymsci.2013.05.008
25. Krikorian V, Pochan DJ (2003) Poly (l-Lactic Acid)/Layered Silicate Nanocomposite: Fabrication, Characterization, and Properties. Chem Mater 15:4317–4324. doi: 10.1021/cm034369+
26. Pluta M, Paul MA, Alexandre M, et al. (2006) Plasticized polylactide/clay nanocomposites. I. The role of filler content and its surface organo-modification on the physico-chemical properties. J Polym Sci Part B Polym Phys 44:299–311. doi: 10.1002/polb.20694
27. Cumkur EA, Baouz T, Yilmazer U (2015) Poly(lactic acid)–layered silicate nanocomposites: The effects of modifier and compatibilizer on the morphology and mechanical properties. J Appl Polym Sci 132:42553. doi: 10.1002/app.42553
28. Scaffaro R, Botta L, Passaglia E, et al. (2014) Comparison of different processing methods to prepare poly(lactid acid)–hydrotalcite composites. Polym Eng Sci 54:1804–1810. doi: 10.1002/pen.23724
29. Mohapatra AK, Mohanty S, Nayak SK (2014) Study of thermo-mechanical and morphological behaviour of biodegradable PLA/PBAT/layered silicate blend nanocomposites. J Polym Environ 22:398–408. doi: 10.1007/s10924-014-0639-x
30. Corcione CE, Frigione M (2012) Characterization of nanocomposites by thermal analysis. Materials 5:2960–2980. doi: 10.3390/ma5122960
31. Kumar M, Mohanty S, Nayak SK, et al. (2010) Effect of glycidyl methacrylate (GMA) on the thermal and morphological property of biodegradable PLA/PBAT blend and its nanocomposites. Bioresour Technol 101: 8406-8415. doi:10.1016/J.biortech.2010.05.075
32. Chow W, Lok S (2008) Thermal properties of poly(lactic acid)/organo-montmorillonite nanocomposites. J Therm Anal Calorim 95:627–632. doi: 10.1007/s10973-007-8975-x
33. Zhang J, Tashiro K, Domb AJ, Tsuji H (2006) Confirmation of disorder α form of poly(L-lactic acid) by the X-ray fiber pattern and polarized IR/Raman spectra measured for uniaxially-oriented samples. Macromol Symp 242:274–278. doi: 10.1002/masy.200651038

34. Monnier X, Delpouve N, Basson N, et al. (2015) Molecular dynamics in electrospun amorphous plasticized polylactide fibers. Polymer 73:68–78. doi: 10.1016/j.polymer.2015.07.047
35. Kar GP, Xavier P, Bose S (2014) Polymer-grafted multiwall carbon nanotubes functionalized by nitrene chemistry: effect on cooperativity and phase miscibility. Phys Chem Chem Phys PCCP 16:17811–17821. doi: 10.1039/c4cp01594k
36. Lacey AA, Price DM, Reading M (2006) Theory and practice of modulated temperature differential scanning calorimetry. In: Modul. Temp. Differ. Scanning Calorim. Springer, pp 1–81
37. Paul MA, Delcourt C, Alexandre M, et al. (2005) Polylactide/montmorillonite nanocomposites: study of the hydrolytic degradation. Polym Degrad Stab 87:535–542. doi: 10.1016/j.polymdegradstab.2004.10.011
38. Chouzouri G, Xanthos M (2007) Degradation of aliphatic polyesters in the presence of inorganic fillers. J Plast Film Sheeting 23:19–36. doi: 10.1177/8756087907076599
39. Feijoo JL, Cabedo L, Giménez E, et al. (2005) Development of amorphous PLA-montmorillonite nanocomposites. J Mater Sci 40:1785–1788. doi: 10.1007/s10853-005-0694-8
40. Pluta M, Galeski A, Alexandre M, et al. (2002) Polylactide/montmorillonite nanocomposites and microcomposites prepared by melt blending: Structure and some physical properties. J Appl Polym Sci 86:1497–1506. doi: 10.1002/app.11309
41. Sinha Ray S, Okamoto K, Okamoto M (2003) Structure−property relationship in biodegradable poly(butylene succinate)/layered silicate nanocomposites. Macromolecules 36:2355–2367. doi: 10.1021/ma021728y
42. Carrasco F, Gámez-Pérez J, Santana OO, et al. (2011) Processing of poly(lactic acid)/organomontmorillonite nanocomposites: Microstructure, thermal stability and kinetics of the thermal decomposition. Chem Eng J 178:451–460. doi: 10.1016/j.cej.2011.10.036
43. Pluta M (2006) Melt compounding of polylactide/organoclay: Structure and properties of nanocomposites. J Polym Sci Part B Polym Phys 44:3392–3405. doi: 10.1002/polb.20957
44. Yeh JT, Tsou CH, Huang CY, et al. (2010) Compatible and crystallization properties of poly(lactic acid)/poly(butylene adipate-co-terephthalate) blends. J Appl Polym Sci 116:680–687. doi: 10.1002/app.30907
45. Lin S, Guo W, Chen C, et al. (2012) Mechanical properties and morphology of biodegradable poly(lactic acid)/poly(butylene adipate-co-terephthalate) blends compatibilized by transesterification. Mater Des 36:604–608. doi: 10.1016/j.matdes.2011.11.036
46. Righetti MC, Gazzano M, Di Lorenzo ML, et al. (2015) Enthalpy of melting of α'- and α-crystals of poly(L-lactic acid). Eur Polym J 70:215–220. doi:10.1016/j.eurpolymj.2015.07.024
47. Zhou Q, Xanthos M (2010) Effects of cationic and anionic clays on the hydrolytic degradation of polylactides. Polym Eng Sci 50:320–330. doi: 10.1002/pen.21520
48. Coiai S, Prevosto D, Bertoldo M, et al. (2013) The chemistry of interfacial interactions in a LDPE-based nanocomposite and their effect on the nano-scale hybrid assembling. Macromolecules, 46:1563−1572 doi.org/10.1021/ma301689h
49. Zhang J, Tashiro K, Tsuji H, et al. (2008) Disorder-to-order phase transition and multiple melting behavior of poly (l-lactide) investigated by simultaneous measurements of WAXD and DSC. Macromolecules 41:1352–1357. doi: 10.1021/ma070607
50. Wei Z, Song P, Zhou C, et al. (2013) Insight into the annealing peak and microstructural changes of poly(L-lactic acid) by annealing at elevated temperatures. Polymer 54:3377–3384. doi:10.1016/j.polymer.2013.04.027

51. Xiao HW, Li P, Ren X, et al. (2010) Isothermal crystallization kinetics and crystal structure of poly(lactic acid): Effect of triphenyl phosphate and talc. J Appl Polym Sci 118:3558–3569. doi: 10.1002/app.32728
52. Xu JT, Wang Q, Fan ZQ (2005) Non-isothermal crystallization kinetics of exfoliated and intercalated polyethylene/montmorillonite nanocomposites prepared by in situ polymerization. Eur Polym J 41:3011–3017. doi: 10.1016/j.eurpolymj.2005.04.042
53. Delpouve N, Saiter A, Dargent E (2011) Cooperativity length evolution during crystallization of poly(lactic acid). Eur Polym J 47:2414–2423. doi: 10.1016/j.eurpolymj.2011.09.027
54. Di Lorenzo ML (2006) Calorimetric analysis of the multiple melting behavior of poly(L-lactic acid). J Appl Polym Sci 100:3145–3151. doi: 10.1002/app.23136
55. Pan P, Kai W, Zhu B, et al. (2007) Polymorphous crystallization and multiple melting behavior of poly(l-lactide): molecular weight dependence. Macromolecules 40:6898–6905. doi: 10.1021/ma071258d
56. Yasuniwa M, Sakamo K, Ono Y, et al. (2008) Melting behavior of poly(l-lactic acid): X-ray and DSC analyses of the melting process. Polymer 49:1943–1951. doi: 10.1016/j.polymer.2008.02.034
57. Kobayashi J, Asahi T, Ichiki M, et al. (1995) Structural and optical properties of poly lactic acids. J Appl Phys 77:2957–2973. doi: 10.1063/1.358712
58. Righetti MC, Tombari E (2011) Crystalline, mobile amorphous and rigid amorphous fractions in poly(L-lactic acid) by TMDSC. Thermochim Acta 522:118–127. doi: 10.1016/j.tca.2010.12.024
59. Passaglia E., Bertoldo M., Ciardelli F., et al. (2008) Evidences of macromolecular chains confinement of ethylene-propylene copolymer in organophilic montmorillonite nanocomposites. Eur Polym J 44:1296–1308. doi: 10.1016/j.eurpolymj.2008.02.011
60. Lu H, Nutt S (2003) Enthalpy relaxation of layered silicate-epoxy nanocomposites. Macromol Chem Phys 204:1832–1841. doi: 10.1002/macp.200350046
61. Yoonessi M, Toghiani H, Kingery WL, et al. (2004) Preparation, characterization, and properties of exfoliated/delaminated organically modified clay/dicyclopentadiene resin nanocomposites. Macromolecules 37:2511–2518. doi: 10.1021/ma0359483
62. Li X, Zhan Z, Peng G, et al. (2011) A new method for preparing completely exfoliated epoxy/clay nanocomposites: nano-disassembling method. Polym Bull 67:719–727. doi: 10.1007/s00289-011-0496-x
63. Mohsen-Nia M, Doulabi FSM (2011) Preparation and characterization of exfoliated poly(vinyl acetate-co-methyl methacrylate)/Cloisite 30B nanocomposite. Polym Bull 68:1663–1675. doi: 10.1007/s00289-011-0665-y
64. Rijal B, Delbreilh L, Saiter JM, et al. (2015) Quasi-isothermal and heat–cool protocols from MT-DSC. J Therm Anal Calorim 121:381–388. doi: 10.1007/s10973-015-4671-4
65. Delpouve N, Arnoult M, Saiter A, et al. (2014) Evidence of two mobile amorphous phases in semicrystalline polylactide observed from calorimetric investigations. Polym Eng Sci 54:1144–1150. doi: 10.1002/pen.23657
66. Pluta M, Galeski A (2002) Crystalline and supermolecular structure of polylactide in relation to the crystallization method. J Appl Polym Sci 86:1386–1395. doi: 10.1002/app.1128
67. Tsuji H, Ikarashi K, Fukuda N (2004) Poly(l-lactide): XII. Formation, growth, and morphology of crystalline residues as extended-chain crystallites through hydrolysis of poly(l-lactide) films in phosphate-buffered solution. Polym Degrad Stab 84:515–523. doi:10.1016/j.polymdegradstab.2004.01.010

68. Shi P, Schach R, Munch E, et al. (2013) Glass transition distribution in miscible polymer blends: from calorimetry to rheology. Macromolecules 46:3611–3620. doi: 10.1021/ma400417f